

# Preliminary Experiment for Validation of Fission Product Flotation System in Passive Molten Salt Fast Reactor

Yun Sik Cho<sup>a</sup>, Hyo Jun Ahn<sup>a</sup>, Do Won Lee<sup>a</sup>, Sung Joong Kim<sup>a,b\*</sup>

<sup>a</sup>Department of Nuclear Engineering, Hanyang University, 222 Wangsimni-ro, Seongdong-gu, Seoul 04763, Republic of Korea

<sup>b</sup>Institute of Nano Science & Technology, Hanyang University, 222 Wangsimni-ro, Seongdong-gu, Seoul 04763, Republic of Korea

\*Corresponding author: sungkim@hanyang.ac.kr

\***Keywords** : MSR, PMFR, Helium Bubbling System, Flotation Experiment, Nano Particle

## 1. Introduction

Liquid Fueled Molten Salt Reactor (MSR), one of the Generation IV reactors, is globally recognized as a reactor with high thermal efficiency and low potential for radioactive material leakage due to the high operating temperature and solidus temperature of molten salt coolant [1]. While MSR has numerous advantages, its molten salt coolant also has a challenge of increased corrosion potential in complex mechanical structures, making it difficult to utilize facilities such as pumps in the primary system [2]. To address the issue of low pump availability resulting from the high corrosion potential in MSR, a Passive Molten-salt Fast Reactor (PMFR) has been developed, which include a chloride-based, long-life natural circulation concept. The PMFR system operates as an integrated reactor based on natural circulation, where thermal energy is generated in the liquid fuel in primary system. As a result of utilizing liquid fuel, fission products are continuously generated within the primary system [3]. Particularly, noble metal-based fission products such as Mo, Te, Ru, Rh, Pd, Se, etc among them may not be dissolved in the molten salt coolant, potentially causing local corrosion, fouling, or instability in reactor power distribution within the primary system. Existing MSR systems have proposed a methodology involving the application of a helium bubbling system, which can effectively remove noble fission products from the core by their high adsorption potential to helium bubbles and be connected to an online reprocessing system [4,5,6]. However, due to the system-integrated natural circulation concept of PMFR, the existing online reprocessing system cannot be applied. Therefore, it is necessary to develop a modified design concept to introduce a Flotation system into the PMFR reactor. Consequently, the objective of this study is to develop the concept of a modified Flotation system, replacing the existing helium bubbling system, and experimentally validate its effectiveness.

## 2. Methods and Results

### 2.1 Helium Bubbling System in PMFR

The concept of the helium injection flotation system proposed in this study is as follows. Firstly, helium gas will be injected at the bottom of the reactor, and noble fission products will adsorb onto the injected helium bubbles. The noble fission products will then be transferred to structure at the top of the primary system by the buoyancy of the helium bubbles. Subsequently, the bubbles will burst at the free surface at the top through the flotation structure. The separated noble fission products will be transported along the structure to the adsorbent, finally resulting in their separation and isolation from the primary system. Fig. 1 illustrates an overview of concept of the Helium Bubbling flotation system in PMFR described above.

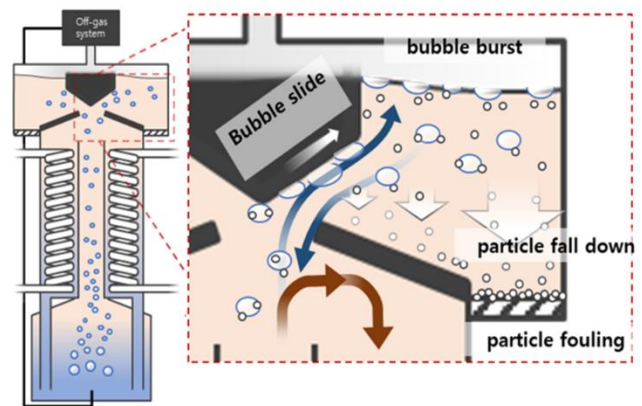


Fig. 1. Conceptual diagram of helium bubbling in Passive Molten Salt Fast Reactor

### 2.2 Experimental Description

In this study, a scaled-down similarity experiment was conducted to experimentally verify the effectiveness of the Helium Bubbling flotation system in PMFR. The 1/4 cylindrical experimental apparatus was equipped with a nozzle at the bottom for helium injection and comprised a riser where bubbles were injected to interact with nanoparticles, and an upper flotation structure. One inch pipes were connected between the top and bottom to facilitate natural circulation driven by buoyancy of bubbles. Flow meters and thermocouple were installed to monitor flow rate and temperature, and a visualization window was included to observe 3D bubble dynamics. The experiment involved dissolving Molybdenum (Mo)

nanoparticles which is one of the representative noble fission products in MSR, into the system. The changes in concentration within the system and above the structure were observed for each 20 minutes. Inductively Coupled Plasma Mass Spectrometry (ICP-MS) measurements were conducted to observe concentration changes quantitatively by measuring the mass of Mo particles within the sample. The experimental procedure was summarized in Fig. 2.

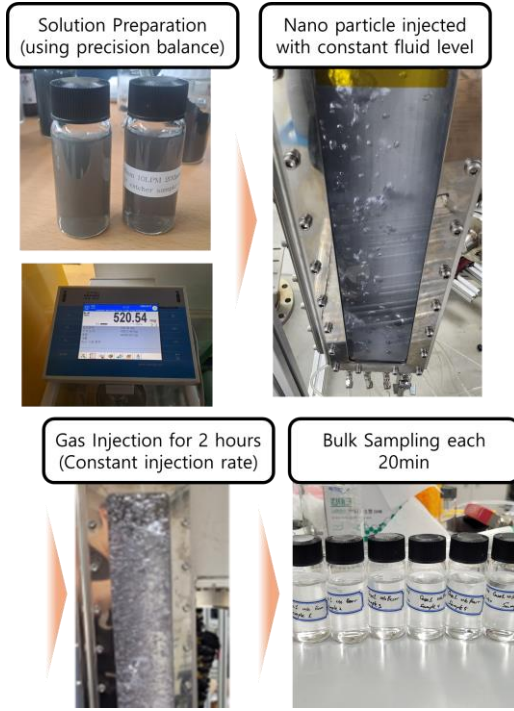


Fig. 2. Schematics of experimental procedures

### 2.3 Quantification of Flotation Process

In addition to the experiment, an Analytic Solution was derived for the analysis of the experimental results in this study. The interaction process between particles and bubbles can be quantified into three each process: Collision, Attachment, and Detachment [7]. First, during bubbles rise, they collide with particles. As the particle concentration increases or the bubble size increases, the probability of collision increases, expressed as collision probability ( $P_c$ ) in the following equation [8]:

$$P_c = \left( \frac{1}{1 + \frac{u_p}{u_b}} \right) \left( \frac{Stk}{Stk + a} \right)^b \left( 1 + \frac{D_p}{D_b} \right)^2 \quad (1)$$

where  $u_p$  is the particle settling velocity,  $u_b$  is the bubble rising velocity,  $D_p$  is the particle diameter, and  $D_b$  is the bubble diameter.

Subsequently, the collided bubble and particle have attachment probability ( $P_a$ ), which is proportional to facing time between the bubble and particle and influenced by turbulence represented by Reynolds number [9].

$$P_a = \sin^2 \left[ 2 \tan^{-1} \exp \left( - \frac{45 + 8Re^{0.72} u_b t_i}{15D_b \left( \frac{D_b}{D_p} + 1 \right)} \right) \right] \quad (2)$$

Here,  $t_i$  is the induction time which means collision time.

The collided bubble and particle also have a detachment probability ( $P_d$ ). The detachment probability can be calculated from the force balance between attachment and detachment force including surface tension of the bubble, gravitational force, hydrostatic pressure, etc. [10, 11]

$$P_d = \frac{1}{1 + \frac{F_{attach}}{F_{detach}}} \quad (3)$$

$$\frac{F_{attach}}{F_{detach}} \approx \frac{3(1 - \cos \theta_d) \gamma}{g \left( \rho_p - \rho_w \left( 1/2 + 3/4 \cos \left( \frac{\theta_d}{2} \right) \right) \right)} \frac{1 + \frac{D_p}{D_b}}{D_p^2} \quad (4)$$

where  $\gamma$  is the surface tension, and  $\theta_d$  is the contact angle between the particle and the bubble.

### 2.4 Visualization of Bubbles in Experimental Loop

As mentioned earlier, the objective of this study is not only to derive analytic solutions through Equations (1)-(4) but also to compare and analyze these solutions with the experimental results. To derive these analytic solutions, information such as the rising velocity and size of bubbles and the flow rate of the liquid is required.

To obtain the information, experimental facilities was constructed with a visualization window to observe images of bubble dynamics. The behavior of bubbles within the channel was observed using a high-speed camera. Representative images showing fully observable bubble dynamics were extracted, and from specific frames, the frequency distribution of each size of bubble were determined. Additionally, by deriving the distance traveled per several frames, the rising velocity of the bubbles was also determined. The results summarized in Figure 3 indicate the distribution of bubble sizes and their rising velocities varying with each gas injection rate. The diameter of the bubbles was observed to increase linearly, approximately measuring 4.6, 6.4, and 8.7 mm, corresponding with 6, 10, and 14 lpm of the gas injection flow rates, respectively. Meanwhile, the rising velocity of the bubbles were observed to be 0.1699 m/sec, 0.1653 m/sec, and 0.1726 m/sec, respectively, showing no significant correlation between the gas injection flow rate and the bubble's rising velocity.

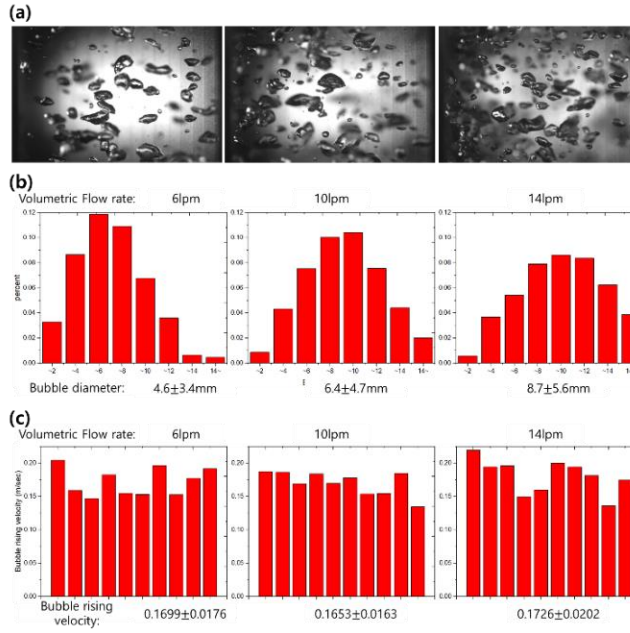


Fig. 3. (a) bubble images captured by a high-speed camera and summary of distribution of (b) bubble diameters and (c) bubble rising velocities for each gas injection flow rates

### 3. Result

Table 1 provides a summary of the experiments conducted in this study. Three variables mainly affecting the efficiency of noble nanoparticle removal through helium injection were chosen: gas injection rate, size and initial concentration of nanoparticle. Significant variations were introduced in these three variables, and experiments were iteratively repeated three times to ensure the reliability of the results.

Table I: Test Matrix for Flotation Experiment

Case	Gas injection rate (lpm)	Particle size (nm)	Initial Concentration (ppm)
Base Case	10	40	11
1	6	40	11
2	14	40	11
3	10	500	11
4	10	40	1.1
5	10	40	110

Fig. 4,5,6 summarizes the experimental results conducted in this study. As mentioned earlier, the experiments were repeated three times, and the mass of nanoparticles extracted from the system was quantitatively determined using ICP-MS. Additionally, the experimental results in the following graph were plotted by converting the concentration of particles extracted before and after the experiments into a percentage change according to the following equation.

$$\text{Decrease Rate} = \frac{C_{init} - C_{final}}{C_{init}} \quad (5)$$

Figure 4 summarizes the variation in decrease rate as a function of gas injection rate. The experimental results presented in Fig. 4 was shown that the linear decrease rate increased proportionally with the increase in gas injection rate. Referring to the graph in Fig. 3, it was noted that as the gas injection rate increased, the diameter of the bubbles also increased. With an increase in bubble diameter, the cross-sectional area for bubbles to encounter particles increased, but the potential for bubbles to adsorb particles decreased. However, it is estimated that the absolute number of bubbles also increases with the increase in gas flow rate, leading to a gradual increase in bubble removal efficiency.

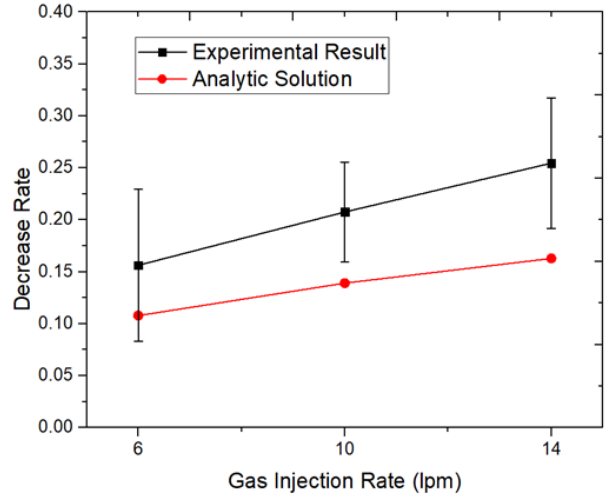


Fig. 4. Experimental result for each gas injection rate

Figure 5 presents the difference in decrease rates in experiments conducted using nanoparticles of 40 and 500 nm, respectively. The results shows that there was a significant increase in the removal rate observed in the experiment using 500 nm nanoparticles compared to the one employing 40 nm nanoparticles. However, according to Brownian motion dynamics of nanoparticles, it is assumed that this increase in removal rate is not due to particle removal through the flotation process. According to previous studies [12], for noble nano fluids, as the particle size decreases sufficiently, the behavior of the particles follows an increasing potential of Brownian motion. Based on this study, as evident from the Brownian diffusivity equation below, it can be observed that the Brownian diffusion potential increases as the particle size decreases.

$$D = \frac{k_B T}{6\pi\mu r} \quad (6)$$

Under the experimental conditions conducted in this study, it is estimated that a significant amount of particles

may have been lost due to sedimentation both before and after the experiment.

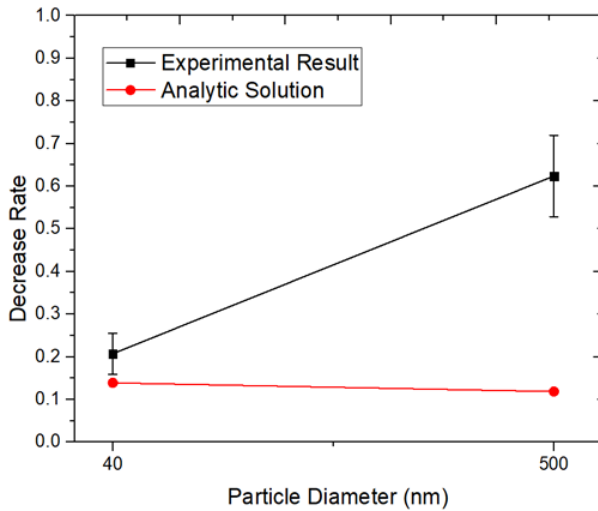


Fig. 5. Experimental result for each particle size

Fig. 6 shows the particle removal rate as a function of concentration change. A significant variation was also observed with concentration change; however, in the experiment with an initial concentration of 1.1 ppm, the quantity was too negligible, making it difficult to maintain a uniform concentration within the system. Consequently, a very high measurement error was observed in the 1.1 ppm experiment. On the other hand, the experiment with an initial concentration of 110 ppm was not fully executed; the measured initial concentration was approximately 53 ppm, instead of the intended 110 ppm. This result indicates that a significant amount of Mo particles at 110 ppm were not completely diluted due to saturation in the solution.

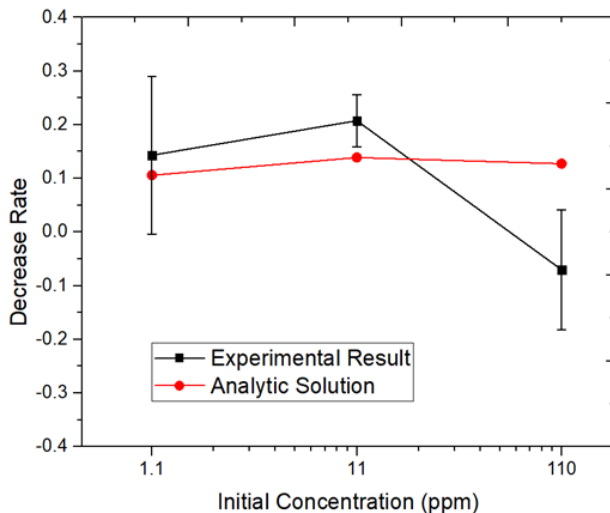


Fig. 6. Experimental result for each initial concentration

Each of the experimental results was also compared and analyzed with the analytic solution as previously mentioned. It was observed that regardless of the changes in gas injection rate, particle size, or

concentration, the results exhibited a common high error in decrease rate when compared to the analytic solution. This is estimated to be due to the characteristic of Mo nanoparticles easily dissolving in the fluid, while the characteristic of noble metals leads to be slowly segmentate. Since the calculations by the analytic solution only consider removal by flotation under the assumption that nanoparticles are completely dissolved in the fluid, it was expected that the assumption makes high errors.

#### 4. Conclusions

This study aims to experimentally verify the Helium Bubbling System for noble fission products removal which is a characteristic of liquid fueled MSR. Especially, the objective of this study was to evaluate the applicability of the Helium Bubbling System to PMFR of system-integrated characteristics. Additionally, the study includes sensitivity analyses which presented significant effect of gas injection rate, particle size, and concentration on the efficiency of noble nanoparticle removal through flotation. The analysis revealed a proportional relationship between gas injection rate and removal efficiency, with larger bubble diameters potentially leading to decreased adsorption potential despite increased surface area. Additionally, particle size variation cannot demonstrate decrease by removal rate, because of low Brownian diffusion potential of particle size 500nm case. Furthermore, concentration changes exhibited inconsistent variations, with extremely high concentrations above saturation concentration of 110ppm case. The comparison with analytical solutions showed large error because of the absence of sedimentation effects in analytic solution. The results and comparison with analytic solution give the necessity not only for accurately assessment nanoparticle concentration changes, but also for the development of analytic solutions including sedimentation effect in future studies.

#### 4. Acknowledgment

This research was supported by the National Research Foundation of Korea (NRF) and funded by the ministry of Science, ICT, and Future Planning, Republic of Korea (grant numbers NRF-2021M2D2A2076382). This work was supported by the National Research Foundation of Korea (NRF) grant funded by the Korea government (MSIT) (RS-2023-00261295)

#### REFERENCES

- [1] J. Serp, M. Allibert, O. Beneš, S. Delpech, O. Feynberg, V. Ghetta, D. Heuer, D. Holcomb, V. Ignatiev, J. L. Kloosterman, L. Luzzi, E. Merle-Lucotte, J. Uhlír, R. Yoshioka and D. Zhimin, "The molten salt reactor (MSR) in generation IV: overview and perspectives," *Progress in Nuclear Energy*, Vol. 77, pp. 308-319, 2014.

- [2] P. Sabharwall, M. Ebner, M. Sohal, P. Sharpe, M. Anderson, K. Sridharan, J. Ambrosek, L. Olson, P. Brooks, "Molten Salts for High Temperature Reactors: University of Wisconsin Molten Salt Corrosion and Flow Loop Experiments--Issues Identified and Path Forward," No. INL/EXT-10-18090, Idaho, USA, 2010.
- [3] R. J. Kedl, "Migration of a class of fission products (noble metals) in the Molten-Salt Reactor Experiment," No. ORNL-TM-3884, Oak Ridge, Tennessee, USA, 1972.
- [4] D. Journée, "Helium bubbling in a molten salt fast reactor," pp. 7-12, TU delft, Zuid-Holland, Nederlands, 2014.
- [5] E. Cervi, S. Lorenzi, L. Luzzi, "Multiphysics analysis of the MSFR helium bubbling system: A comparison between neutron diffusion, SP3 neutron transport and Monte Carlo approaches," *Annals of Nuclear Energy*, Vol. 132, pp. 227-235, 2019.
- [6] E. Cervi, S. Lorenzi, A. Cammi, L. Luzzi, "Development of an SP3 neutron transport solver for the analysis of the Molten Salt Fast Reactor," *Nuclear Engineering and Design*, Vol. 346, pp. 209-219, 2019.
- [7] Ralston, John, Daniel Fornasiero, and Robert Hayes, "Bubble-particle attachment and detachment in flotation," *International Journal of Mineral Processing*, Vol. 56, Nos. 1-4, pp. 133-164, 1999.
- [8] R.H. Yoon, "The role of hydrodynamic and surface forces in bubbleparticle interaction," *International Journal of Mineral Processing*, Vol. 58, No. 1, pp. 129-143, 2000.
- [9] V.e. Ross, "Particle-bubble attachment in flotation froths," *Minerals Engineering*, Vol. 10, No. 7, pp. 695-706, 1997.
- [10] H. Schulze, *Physico-chemical Elementary Processes in Flotation, An Analysis from the Point of View of Colloid Science including Process Engineering Considerations*, Elsevier, 1984.
- [11] R Ralston, "Bubble particle attachment and detachment in flotation," *International Journal of Mineral Processing*, Vol. 56, pp. 133-164, 1999.
- [12] Schmidt, J. R., and J. L. Skinner, "Hydrodynamic boundary conditions, the Stokes-Einstein law, and long-time tails in the Brownian limit," *The Journal of Chemical Physics*, Vol. 119, No. 15, pp. 8062-8068, 2003.